Computational and Spectroscopic Studies of Dichlorofluoroethane Hydrate Structure and Stability

Jeffery A. Greathouse* and Randall T. Cygan

Sandia National Laboratories, Albuquerque, New Mexico 87185-0754

Robert W. Bradshaw, Eric H. Majzoub, and Blake A. Simmons

Sandia National Laboratories, Livermore, California 94551

Received: April 16, 2007; In Final Form: August 31, 2007

Clathrate hydrates consisting of HCFC (hydrochlorofluorocarbon) guest molecules within host water cages represent a promising new medium for water desalination. The HCFC used in this study, 1,1-dichloro-1-fluoroethane (R141b), forms a structure II hydrate phase at mild conditions (0 °C, 0 atm). We present a detailed molecular picture of the structure and dynamics of guest R141b molecules within water cages, obtained from ab initio calculations, molecular dynamics simulations, and Raman spectroscopy. Such information will be needed to understand and control the nucleation and growth of these hydrates for industrial applications. Density functional theory calculations were used to provide an energetic and molecular orbital description of R141b stability in both large and small cages in a structure II hydrate. Additionally, the hydrate of an isomer, 1,2-dichloro-1-fluoroethane, does not form at ambient conditions due to extensive overlap of electron density between guest and host. Results for the isomer hydrate were supported by classical molecular dynamics simulations and synthesis attempts. Molecular dynamics simulations show that R141b hydrate is stable at temperatures up to 265 K, while the isomer hydrate is only stable up to 150 K. Despite hydrogen bonding between guest and host, R141b molecules rotate freely within the water cage. The Raman spectrum of R141b in both the pure and hydrate phases is also compared with vibrational analysis from both computational methods. In particular, the frequency of a carbon−halogen stretch mode (585 cm^{-1}) undergoes a shift to higher frequency in the hydrate phase. Raman spectra also indicate that this peak undergoes splitting and intensity variation as the temperature is decreased from +4 to −4 °C.

Introduction

Clathrate compounds consist of a solid framework of host molecules that surround guest molecules. The term clathrate hydrate applies when water is the host molecule, and clathrate hydrates are characterized by forming conditions of temperature ≤ 0 °C and pressure ≥ 1 atm.[1] Structure I hydrates consist of two types of water cages: a small cage consisting of 20 water molecules and denoted 5^{12} and a large cage consisting of 24 water molecules ($5^{12}6^2$). Structure II hydrates also have the 20-water small cages as well as large 28-water cages ($5^{12}6^4$). In both structure I and structure II hydrates, water molecules maintain tetrahedral coordination through four hydrogen bonds per molecule, as in hexagonal ice. The molecular diameter of a guest molecule determines the appropriate cage and therefore the type of hydrate formed.[1] Clathrate hydrates consisting of natural gas guest molecules (e.g., methane) have received attention as a potential energy source, although pressures greater than 20 atm and temperatures near 273 K are required for hydrate stability.[2]

Clathrate hydrates can form in the presence of dissolved solutes and therefore have potential use in water desalination processes. Guest molecules considered for this application include propane[3] and chlorofluorocarbons.[4,5] However, many complex and fundamental issues remain to be solved before hydrate desalination can be considered as a commercial technology. Specifically, hydrate nucleation, growth, and crystal agglomeration must be understood. In the presence of dissolved solute, trapped solute and recovery of pure water from a hydrate phase must also be considered. Using computational and spectroscopic techniques, our aim is the characterization of guest−water interactions at the molecular level to aid in understanding the more complex issues associated with the hydrate desalination process.

Experimental studies of the structure and phase equilibria of gas hydrates formed by chlorofluorocarbons and other large guest molecules have been reviewed elsewhere.[1,6−9] However, Raman spectroscopic techniques have been used recently to better understand guest−host interactions at the molecular level.[10−12] Comparisons between spectroscopic and computational techniques will enable more effective use of gas hydrates in industrial applications. Computational studies of gas hydrates typically include as guest molecules either methane[13−25] or hydrogen[21,26,27] because of their potential use in energy storage and production. The guest is usually treated as a single Lennard-Jones particle,[17,19,20,22−24,28] although atomistic models for both methane[13,15] and hydrogen[26,27] have been published. In some cases, ab initio calculations have been performed, and guest−water interaction parameters were derived for classical simulations.[18,21,28,29] Simulation techniques have also been used to study the thermodynamics of hydrate formation and dissociation, although simulation time scales of at least 10 ns are

* To whom correspondence should be addressed. E-mail: jagreat@sandia.gov.

10.1021/jp072968o CCC: $37.00
Published on Web 10/16/2007

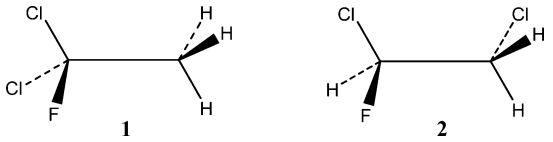

Figure 1. Hydrate formers considered in this work: **1** (1,1-dichloro-1-fluoroethane, R141b) and **2** (1,2-dichloro-1-fluoroethane).

typically needed,[19,22,23,25] and effects of finite system sizes should also be considered.[14]

The classical simulation approach used in this study follows from previous work in which a general force field for organics (consistent valence force field, CVFF)[30] was used to calculate thermal expansion parameters and vibrational spectra of methane hydrate.[16] The advantage of a general force field is its transferability to new hydrate systems without the need to derive new water−guest interaction parameters. In this paper, we use molecular simulation techniques to examine the structure and stability of gas hydrates formed from two isomers of dichlorofluoroethanes. One of these isomers, 1,1-dichloro-1-fluoroethane (R141b, **1** in Figure 1), is being considered as a hydrate former in water desalination processes.[31] Its high heat capacity and mild hydrate-forming conditions (0 °C, 75 mbar)[6] make R141b an ideal candidate for low-energy water desalination. Additionally, we compare simulated vibrational spectra with Raman spectra to investigate changes in R141b vibrational frequencies before and after formation of the hydrate phase. United States law now prohibits the production or importation of R141b, but we chose it on the basis of the availability of experimental data on R141b hydrates.[6,8,32−34] Industrial applications of hydrates made from trihaloethanes will include refrigerants that are allowed under current law.

Methods

Due to their size, dichlorofluorohaloethanes form structure II hydrates, where we assume an occupancy of one molecule in each of the eight large cages. The 16 small cages are empty in the pure hydrate, but smaller guest molecules such as methane could be included in the small cages. Cavity diameters for accommodation of guest molecules have been estimated at 6.7 and 5.0 Å for the large and small cages, respectively.[1]

Density Functional Theory (DFT) Methods. Electronic structure calculations for cluster models of the structure II large ($5^{12}6^4$) and small (5^{12}) hydrate cages with the R141b molecule were completed using the density functional code DMol^3.[35,36] Because atomic coordinates were not provided with the crystal structure data for R141b hydrate,[6] we chose to use both the coordinates and lattice parameter of a mixed gas hydrate (structure II, space group $Fd3m$, $a = 17.192$ Å), with Xe atoms occupying the small cages and CCl_4 molecules occupying the large cages.[37] This lattice parameter is very close to 17.234 Å reported for R141b hydrate.[6] We are confident that 17.192 Å is an adequate estimate of the R141b hydrate lattice parameter for the DFT calculations. Hydrogen positions of the water molecules were classically optimized as described below. All-electron configurations were obtained for the geometry-optimized R141b molecule within each hydrate cage with fixed positions for the water molecules. Similar calculations were performed for the isomer (1,2-dichloro-1-fluoroethane, **2** in Figure 1; *gauche* and *anti* configurations) to determine the relative energies and suitability as a hydrate-forming compound. Calculations incorporated the nonlocal gradient-corrected or generalized gradient approximation, with double numerical plus polarization (DNP) functionals to ensure a proper description of hydrogen bonding for the water and organic molecules.[38] The DNP basis set includes a second set of valence atomic orbitals beyond the minimal basis, plus polarization orbitals involving d-functions for non-hydrogen atoms and p-functions for hydrogen atoms.[35] This numerical basis set provides the highest accuracy for the electronic structures calculated for the selected hydrate models. Iteration of the wave equations to a self-consistent field solution required an energy difference of less than 0.0063 kJ·mol^{-1}. Energy-minimized structures were derived through a series of steepest descent, conjugate gradient, and Newton−Raphson methods, allowing all atoms to relax during the optimization. An energy convergence criterion of 0.013 kJ·mol^{-1} was used for the geometry optimization of the dichlorofluoroethane while the water molecules were kept constrained to their observed structural positions.

A similar computational approach was used to examine the electronic structure of crystalline models of the R141b hydrate and isomer hydrate systems. The periodic simulation cells were equivalent to the isometric structure II unit cell with 136 water molecules, 8 dichlorofluoroethane molecules occupying each of the large cages, and vacant small cages. Wave functions were calculated using a single integration in reciprocal space (Γ point). The cell parameter ($a_o = 17.192$ Å) was held constant for constant-volume conditions during the optimization, and no symmetry was imposed on the atomic positions ($P1$ space group). In contrast to the cluster calculations, all atomic positions were relaxed during the optimization of the periodic models.

Vibrational spectra for the cluster models of R141b and R141b hydrate were derived using the standard approach of Wilson[39] in which the components of the second derivative of the energy (Hessian matrix **F**) are used to derive harmonic frequencies

$$F_{ij} = \frac{1}{(m_i m_j)^{1/2}} \frac{\partial^2 E}{\partial q_i \partial q_j} \tag{1}$$

where m_i and m_j are atomic masses and q_i and q_j are Cartesian coordinates associated with atoms i and j. The frequencies are equivalent to the square roots of the eigenvalues of **F**. Finite differences of the analytical first derivatives of the energy are used to derive the Hessian matrix. This is accomplished by a series of single-point energies that are obtained as each atom in the system is displaced by 0.01 bohr in each direction. Spectral intensities for each mode are proportional to the square of the atomic polar tensor. Lorentzian-shaped peaks with 5.0 cm^{-1} full width at half-maximum were derived from the calculated frequencies. No attempt was made to derive vibrational spectra for the crystalline models using this method due to computational cost. Additionally, the calculated vibrational spectra involving the hydrate cages are only approximate representations of the cluster dynamics because the water molecule positions were constrained to best represent the local water cage structure. Power spectra derived from velocity autocorrelation methods with classical simulations are closely related to the spectra obtained through the Hessian analysis of electronic structure results. Classical methods rely on kinetic energy to statistically sample accessible regions of the potential energy surface over long simulation times at a particular temperature, while the dynamical matrix in normal model analysis directly samples the electronic-based internal energy surface at 0 K.

Classical Molecular Dynamics. Classical simulations were performed with the open force field module of Cerius^2 (Accelrys, Inc.) using CVFF.[30] Intermolecular potential parameters between organic guest atoms (C, H) and host water molecules

(simple point charge model[40]) were obtained from geometric combination rules upon which CVFF is based. CVFF has previously been shown to provide accurate structural results for methane hydrate,[16] and here we apply similar techniques to more complex trihaloethane guests. Because CVFF includes molecular flexibility for both water and guest molecules, we were able to calculate vibrational power spectra from atomic velocity autocorrelation functions.[41] Potential energy interactions include intramolecular (bond, angle, torsion) as well as intermolecular (electrostatic, van der Waals) terms. A real-space cutoff value of 10.0 Å was used for intermolecular interactions, and Ewald summation[41] with a precision of 4×10^{-4} kJ·mol^{-1} was used for long-range electrostatic interactions. Initial simulations were performed in the constant *NPT* (N = number of particles, P = 0 atm pressure, T = temperature) ensemble to obtain average supercell volume and lattice parameters. Subsequent simulations to obtain structural and vibrational data were preformed in the constant *NVT* (V = volume) ensemble using an equilibrated *NPT* configuration with lattice parameters equal to their average values at that temperature. Barostat and thermostat relaxation times were 0.5 and 0.1 ps, respectively. All force field parameters, including atomic charges, were taken directly from CVFF.[30] The time step for all simulations was 0.25 fs.

Our primary interest is R141b hydrate, **1**, but to examine the effect of molecular size on hydrate stability, we also considered isomer **2**. For the computational portion of this study, we only considered the *S*-enantiomer of **2**. Due to the symmetry of the water cage, we would not expect different structural or vibrational results if we had used the *R*-enantiomer. The initial configuration of water O atoms was the same as that used for the DFT calculations. The initial positions of H atoms were determined by a series of energy minimizations with immobile O atoms, which resulted in a hydrogen-bonded network of water cages. Although the unit cell dipole moment is not zero in our initial configuration, the Bernal−Fowler rules[42] are satisfied. Macroscopic system sizes would be needed to obtain a dipole moment of zero, and the thermal energy at the temperatures used in our MD simulations causes the net dipole moment to fluctuate. In fact, we observe rotations of water molecules during these simulations, which causes a cascade effect of hydrogen bond breaking and re-forming and associated changes in the dipole moment. A supercell was created consisting of eight unit cells in a $2 \times 2 \times 2$ expansion, with an initial lattice parameter of 34.384 Å. The supercell contained 1088 water molecules, 64 large cages, each occupied by a guest (**1** or **2**), and 128 empty small cages. The trihaloethane molecules were placed randomly within the large cages while overlap of atomic van der Waals radii was avoided.

The temperature ranges of stable hydrates were determined by performing anisotropic *NPT* simulations 1000 ps in length. R141b hydrate was stable at temperatures up to 265 K. Above 265 K, the hydrate system dissociates into an aqueous phase and an organic phase. The isomer hydrate is stable only at temperatures below 150 K. Because periodic models of solids lack a surface nucleation site, solid phases such as ice can be stable at temperatures well above the simulated melting temperature.[43] Therefore, 265 and 150 K should be considered as upper limits for the thermal stability of hydrates with guests **1** and **2**, respectively. We have not identified a published melting temperature of ice Ih using the flexible SPC water model, but the simulated melting temperatures of ice Ih using the rigid SPC and SPC/E water models have been reported as 190 and 215 K, respectively.[44] Using the SPC/E water model, ice Ih was found to be stable in *NPT* Monte Carlo simulations up to 295 K, which is 80 K above its transition temperature.[43] It is therefore likely that the simulated dissociation temperatures for hydrates of **1** and **2** using our hybrid force field are significantly lower than 265 and 150 K. However, on the basis of our desire to match the theoretical and experimental conditions, further simulations were carried out in the *NVT* ensemble with T = 265 K. The initial configuration was taken from the equilibrated *NPT* configuration of R141b hydrate at 265 K. Lattice parameters (a_0, b_0, c_0) were 34.28, 34.54, and 33.92 Å, respectively, which correspond to average values from the *NPT* simulation at 265 K. One set of simulations were performed in which the waters were completely mobile. However, since the isomer hydrate is not stable at 265 K, a second set of simulations were performed in which the water molecules were held in fixed positions on the basis of their initial configuration. In this way, comparisons were made between hydrates of both **1** and **2**. Initially, *NVT* simulations 40 ps in length were used to obtain structure and vibrational data, but longer simulations 1000 ps in length were used to further investigate guest rotational mobility within the cages. For the 40 ps simulations, RDF data were updated every 50 fs, and velocities were stored every 4 fs. Power spectra of R141b hydrate (mobile water molecules) were obtained by taking the Fourier transform of the velocity autocorrelation functions (VACFs) for each atom type. A VACF window of 20 fs was used, which was also utilized to obtain power spectra of methane hydrate.[16] For comparison, power spectra were also obtained from 40 ps *NVT* simulations of hexagonal ice and pure R141b at 265 K. For ice Ih, the supercell contained 360 molecules. The model system for pure R141b corresponded to a pressure of 300 kbar at 265 K (120 molecules in a cubic supercell of dimension 20.0 Å).

Hydrate Synthesis and Characterization. A stirred thermostatic pressure cell was used to synthesize R141b (CAS 1717-00-6) hydrate, as described elsewhere.[31] Hydrate samples were prepared at approximately 3 °C and atmospheric (total) pressure using R141b hydrate seed crystals, prepared separately by flash freezing, to facilitate rapid hydrate growth. Attempts to make hydrate samples of the isomer (CAS 430-57-9) (**2**) were unsuccessful. Approximately 1 g of the isomer was placed in test tubes along with 5 mL of water. Trials were conducted simultaneously with homogeneous nucleation and secondary nucleation using a few milligrams of R141b hydrate seed crystals. Comparable tubes with R141b were prepared as controls. The test tubes were placed in a conventional refrigerator for at least 3 days at 3 °C and periodically agitated, but no hydrate phase was observed for the isomer, although R141b hydrates were formed. The temperature was subsequently reduced to just above 0 °C, but no hydrates of the isomer were detected. Raman spectra were collected using an Acton (Princeton Instruments) 0.75 m SpectraPro 2750 triple grating spectrograph, with the 532 nm line from a Spectra-Physics Excelsior CW diode-pumped Nd:YAG. Collection times for the hydrate and the R141b reference were 10 and 1 s, respectively, with a power at the sample of approximately 10 mW. Hydrate samples and the R141b reference were held at approximately 0 °C on a thermoelectric cold plate during data collection. The spectra were calibrated using a 20-point neon spectrum. Data were fitted for peak locations with pseudo-Voigt and/or Gaussian peak shapes, using FITYK 0.7.5 (www.unipress.waw.pl/fityk).

Results

DFT Methods. A comparison of the energies obtained from the DFT calculations for the various clathrate systems is presented in Table 1. Due to the difficulty in DFT methods in

TABLE 1: Energies of Water, Guests, and Clathrates Derived from DFT

	no. of H_2O molecules	potential E (kJ·mol^{-1})	ΔE_{form} (kJ·mol^{-1})
Cluster Models			
water molecule	1	−200 682	
R141b		−2 883 584	
1,2-dichloro-1-fluoroethane (*gauche*)		−2 883 573	
1,2-dichloro-1-fluoroethane (*anti*)		−2 883 577	
small cage	20	−4 014 219	
large cage	28	−5 619 886	
R141b in small cage	20	−6 897 642	+161
R141b in large cage	28	−8 503 679	−209
isomer in large cage (*gauche*)	28	−8 503 661	−201
isomer in large cage (*anti*)	28	−8 503 646	−184
Periodic Models			
R141b in large cage	136	−50 371 742	−4743
isomer in large cage (*gauche*)	136	−50 371 594	−4682

reproducing dispersion-related effects in intermolecular systems, caution must be used in interpreting the results of the optimized cluster and periodic systems. Results from the cluster models demonstrate the size restrictions associated with the incorporation of R141b or other similarly sized guest molecules in the small hydrate cage. The formation energy for R141b in the optimized large water cage—presented here relative to the water cage structure—indicates a stability of −209 kJ·mol^{-1} in contrast to +161 kJ·mol^{-1} for R141b in the small cage.

Figure 2 provides a graphical comparison of the electron density derived from the calculations and clearly shows significant overlap of the organic molecule with the water molecules of the small cage leading to this destabilization. Electron density derived for the large cage model shows the isolated R141b electron density distinct from that associated with the water molecules, which exhibit several pairs of prominent hydrogen bonds within the plane of the electron density map. The formation energies for the clathrate cluster with *gauche* and *anti* configurations of **2** are slightly less stable than that calculated for the clathrate with **1**. The *gauche* isomer clathrate is more stable than the *anti* isomer even though the isolated *anti* isomer has a lower energy (4 kJ·mol^{-1}) than the *gauche* isomer. This stabilization is primarily due to the ability of the *gauche* isomer to coordinate the chlorine atoms to the nearby water molecules rather than those across the cage that would be limited by the *anti* configuration of chlorine atoms. Calculations for the optimized periodic hydrate models indicate the stability of the R141b hydrate relative to that for the *gauche* isomer by 148 kJ·mol^{-1}·(unit cell)$^{-1}$ (or 61 kJ·mol^{-1} difference in the formation energy). This energy difference is small compared to the potential energy difference observed (kJ·mol^{-1}·(unit cell)$^{-1}$) in the classical simulations for the same two systems (see below). This comparison of simulation results emphasizes the limitation of DFT methods in accounting for intermolecular dispersion for systems such as hydrates involving guest−cage interactions.[45−47] The empirically derived force field parameters used in the classical simulations provide a more accurate evaluation of these electron correlation effects.

It would be insightful to directly compare the cluster and periodic formation energies presented in Table 1 by normalizing the values on a per guest or cage basis. Simply dividing the periodic model values by the number of guest molecules per unit cell indicates a substantial stabilization of the guest molecule in the large cage of the structure II hydrate. However, this approach ignores the complex interactions associated with the occupied cages that share cage faces with other occupied cages;

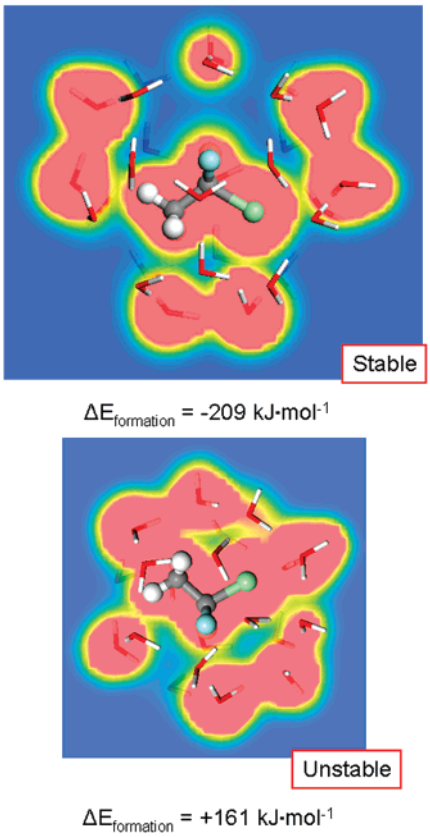

Figure 2. Optimized R141b−water clusters derived from DFT quantum calculations for the large water cage (top) and the small water cage (bottom) of R141b hydrate. The color maps represent the electron density and indicate the presence of destabilizing interactions between coordinating water molecules and the R141b guest in the small cage (top).

each large cage shares faces with four tetrahedrally disposed large cages and their guest molecules. Compared with the formation energies reported in Table 1, which are thermodynamic state values and rigorously determined for multiple reference states, the comparison of periodic and cluster energy values is limited by our inability to fully evaluate the multiple cage−cage, guest−guest, and cage−guest interactions of the periodic models.

The fully optimized periodic hydrate structures provide confirmation of the water oxygen positions observed by McMullan and Kvcik[37] for the structure II hydrate. We observe local perturbations of the oxygen position (∼1.0 Å difference) for about 10% of the water molecules when associated with the organic guest, but overall there is very good agreement for the remaining water oxygen positions (0.22 ± 0.17 Å difference). Additionally, periodic DFT results support the optimized hydrogen-bonding configuration as derived through the classical simulations. Finally, we compared the hydrate-forming abilities of **1** and **2** by calculating the largest "molecular diameter" from the DFT electron density of each molecule. Following the method of Hout and Hehre,[48] a surface contour of 0.002 e·Å^3 was used, which corresponds to van der Waals radii. The calculated molecular diameters were 6.8 Å (**1**) and 7.4 Å (**2**). Using the estimate of 6.6 Å as the "free diameter" inside a large cage of structure II hydrate,[49] it is apparent that isomer **2** is too large to fit inside the large cage of a structure II hydrate.

Classical Molecular Dynamics. All force field simulations discussed below were performed in the *NVT* ensemble at 265 K, with lattice parameters corresponding to the *NPT*-averaged values as discussed previously. We first investigated the effect

TABLE 2: RDF Results for R141b Hydrate (1)

	immobile water			mobile water		
RDF pair[a]	peak max (Å)	peak min (Å)	CN[b]	peak max (Å)	peak min (Å)	CN
Cl−H_w	3.15	3.91	0.71	3.19	3.91	0.70
F−H_w	3.19	3.91	0.34	3.13	3.79	0.29
H−H_w	2.85	3.49		2.93	3.49	
H−O_w	3.04	4.05		3.09	3.99	

[a] H_w and O_w refer to water H and O atoms, respectively. [b] Coordination number calculated at an interatomic distance of 3.0 Å.

TABLE 3: RDF Results for 1,2-Dichloro-1-fluoroethane Hydrate (2)

	immobile water			mobile water		
RDF pair[a]	peak max (Å)	peak min (Å)	CN[b]	peak max (Å)	peak min (Å)	CN
Cl−H_w	2.96	3.75	0.59	3.23	3.93	0.70
F−H_w	2.83	3.57	0.25	3.07	3.71	0.27
H−H_w	3.27			3.19	3.29	
H−O_w	3.53	4.91		3.15	4.41	

[a] H_w and O_w refer to water H and O atoms, respectively. [b] Coordination number calculated at an interatomic distance of 3.0 Å.

of water mobility on guest−host interactions. Radial distribution functions (RDFs) between guest atoms (Cl, F, and H atoms) and water molecules (H_w and O_w atoms) are shown for **1** and **2** in Tables 2 and 3. For R141b (**1**), the Cl−H_w and F−H_w peak data are nearly identical, regardless of water mobility (Table 2). However, Table 3 shows a loss of structure when the isomer (**2**) hydrate is modeled with mobile water molecules. Further comparisons of hydrate structure between **1** and **2** were made on the basis of simulations of immobile water molecules. Figure 3 shows the Cl−H_w and F−H_w RDFs. For **2**, the Cl−H_w and F−H_w peaks are shifted inward by 0.19 and 0.36 Å, respectively. The larger diameter of **2** (7.4 Å compared to 6.8 Å for R141b) results in smaller guest−water distances, as quantified in Table 3 by comparing X−H_w (X = Cl, F) coordination numbers at a distance of 3.0 Å (immobile water molecules). This distance falls within the range of hydrogen bond lengths for both Cl−H_w pairs (2.86−3.21 Å) and F−H_w pairs (2.62−3.01 Å).[50] The larger coordination numbers for **2** again indicate a closer interaction with the water cage due to size constraints. When the isomer hydrate system is simulated with mobile water molecules at 265 K, the hydrate structure dissociates into aqueous and organic phases. Only at much lower temperatures is the isomer hydrate stable. As discussed previously, our calculated molecular diameters for **1** (6.8 Å) and **2** (7.4 Å) suggest that size effects should be considered when the ability of these isomers to form hydrates is being predicted. Finally, we note that the average potential energy of R141b hydrate is approximately 7100 kJ·mol^{-1} lower than that of the isomer. These results highlight the ability of molecular simulations to examine trends in hydrate stability.

We also attempted to quantify the rotational motion of **1** and **2** within the water cages. First, we examined the time dependence of the mean-square displacement (MSD)[41] for both Cl and F atoms in an attempt to see a difference in atomic diffusivity between the isomers. For **1** and **2**, the MSD values reached plateaus after 5.0 ps (data not shown), which is characteristic of solids and not gases or liquids. The plateau value for Cl and F atoms in R141b hydrate (6.3 Å^2) and the isomer (7.4 Å^2) mirrors the difference in van der Waals diameter of the two molecules, which reinforces the concept that the isomer requires a larger volume than is available in a structure II hydrate (Figure 2). Second, the (*x*, *y*, *z*) trajectories of F atoms

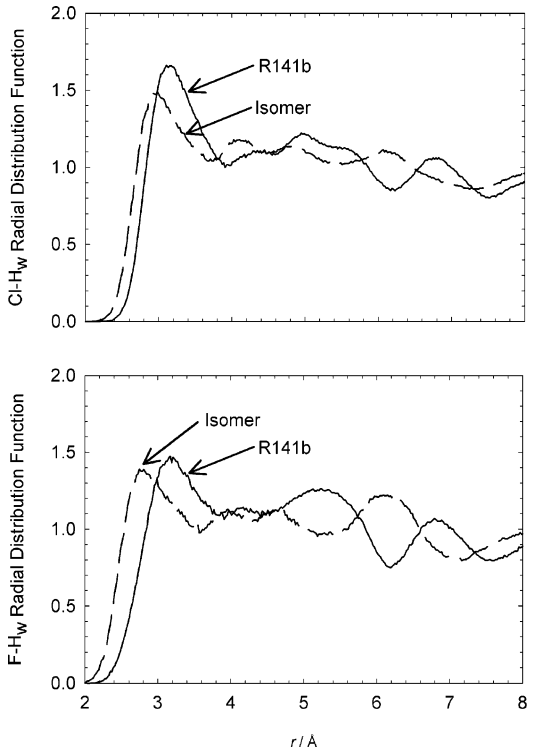

Figure 3. Cl−H_w (upper) and F−H_w (lower) RDFs for R141b hydrate (**1**) and the isomer hydrate (**2**).

in R141b hydrate were plotted, with an example shown in Figure 4. During the shorter simulation of 40 ps, only a portion of the free volume within the cage was sampled by the F atom (Figure 4, top). However, a trajectory from a longer 1000 ps simulation shows that the F atom mapped out the entire free volume of the cage (Figure 4, bottom). The same behavior was seen by both isomers, so we conclude that the difference in hydrate stability between **1** and **2** is caused mainly by intermolecular (hydrogen bonding, van der Waals) interactions due to size effects. The confined space within the large cage did not appear to hinder the rotational motion of either isomer.

Vibrational Analysis of R141b Hydrate. A comparison of the calculated DFT vibrational spectra for the optimized cluster model of R141b and R141b clathrate is provided in Figure 5. Although a scaling factor is often used to correct quantum-based frequencies for comparison to experimental spectra,[45] no such corrections are made in this study; emphasis is placed on the relative changes in the vibrational energy and peak position. Calculations for the cluster model of R141b generated 18 active modes ($3N - 6$, where N = number of atoms) once the molecular translations and rotations were removed. In the mid-infrared region, the R141b spectrum is dominated by C−F and C−Cl stretch modes. Bending modes involving the halogen and carbon atoms occur at lower frequencies (less than 600 cm^{-1}), while those involving C−H bends are observed between 1100 and 1500 cm^{-1}. Stretch modes for C−H occur at the highest frequencies (∼2700 cm^{-1}) and are characterized by relatively small intensities. These spectral features are generally consistent with experimental values as provided by Nakanishi and Solomon.[51]

The calculated spectrum for R141b hydrate is more complex due to the large number of combination modes associated with the large hydrogen-bonding network of water molecules. The spectrum is characterized by a large group of high-frequency O−H stretch modes (2700−3300 cm^{-1}) associated with the water molecules. The associated H−O−H bend modes are

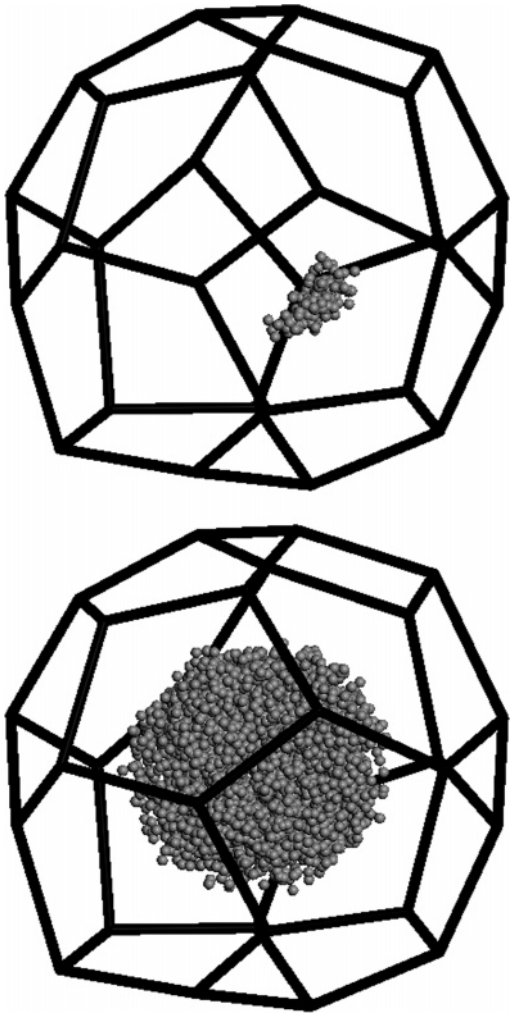

Figure 4. Trajectories (gray spheres) of a fluorine atom in a large cage R141b hydrate during a 40 ps *NVT* simulation (top) and a 1000 ps simulation (bottom) of R141b hydrate. The spheres represent the location of the F atom every 0.25 ps during the simulations. The black lines represent the immobile water cage, with water oxygen atoms at each vertex.

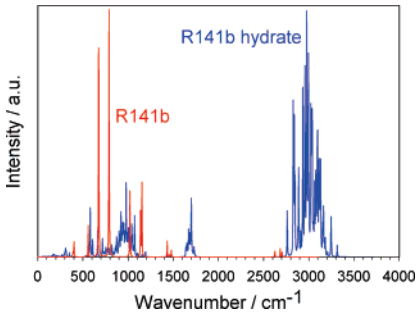

Figure 5. Calculated DFT vibrational spectra obtained from a normal mode analysis of optimized cluster models from DFT for R141b (red) and R141b hydrate (blue).

observed at approximately 1700 cm^{-1}. The libration modes for the water molecules dominate much of the region from 300 to 1200 cm^{-1}, while the relatively small intensities for the R141b molecule within the large cage are observed at 605 and 904 cm^{-1}, respectively, for the C−Cl and C−F stretch modes. Considering the limitations of the DFT method, the calculated spectra are generally consistent with those observed by classical simulation (see below). Animation of the vibrational modes associated with the R141b molecule suggests the symmetric

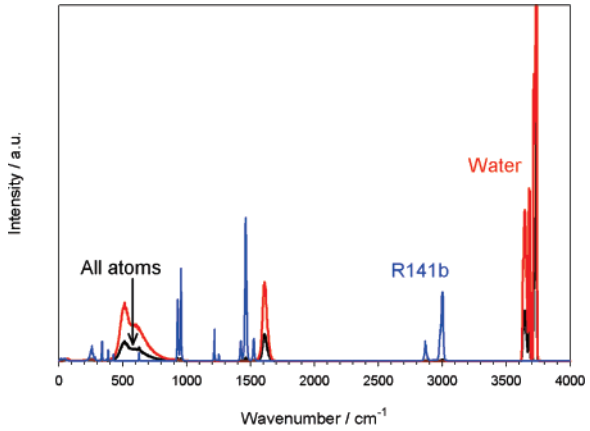

Figure 6. Simulated power spectrum of R141b hydrate (black line), showing contributions from water atoms (red line) and R141b atoms (blue line). Intensities of the R14b peaks were scaled to enhance visibility.

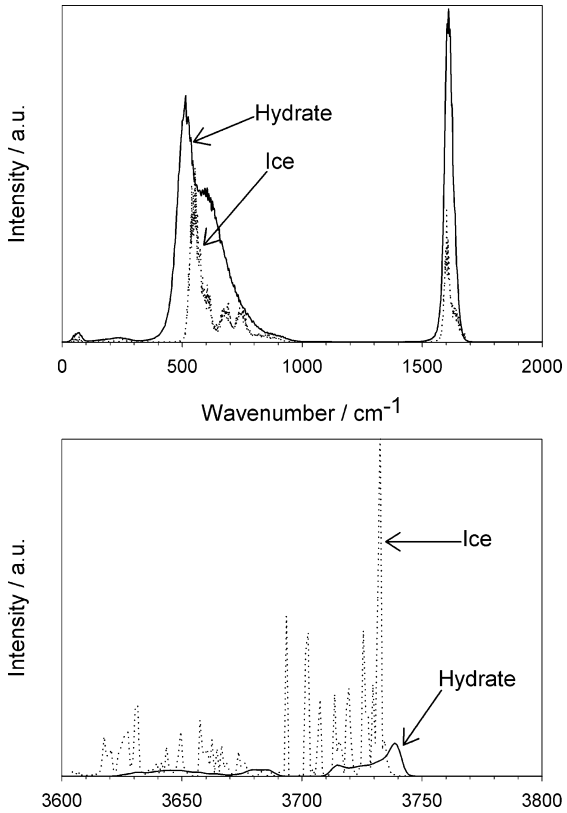

Figure 7. Comparison of power spectra (H atoms only) of R141b hydrate (solid line) and hexagonal ice (dotted line). The intensities at lower frequencies (top) have been amplified for ease of viewing.

carbon−halogen stretch at 559 cm^{-1} is most sensitive to hydration and exhibits a shift to higher frequency.

The vibrational power spectrum of R141b hydrate obtained from the classical molecular dynamics simulations is shown in Figure 6. The overall spectrum is dominated by contributions from water molecules, but peaks due to R141b are visible after rescaling their intensities. The water modes can be classified as follows: O−H stretch (3600−3750 cm^{-1}), H−O−H bend (1500−1700 cm^{-1}), and librations (400−1000 cm^{-1}). Similarly, for R141b, the modes are C−H stretch (2850−3050 cm^{-1}), C−F stretch and CH_3 bend (1400−1550 cm^{-1}), and C−C stretch (1200−1300 cm^{-1}). Several modes between 600 and 1530 cm^{-1} involve both Cl and F atoms, and the mode at 630 cm^{-1} is primarily a symmetric carbon−halogen stretch. The spectrum

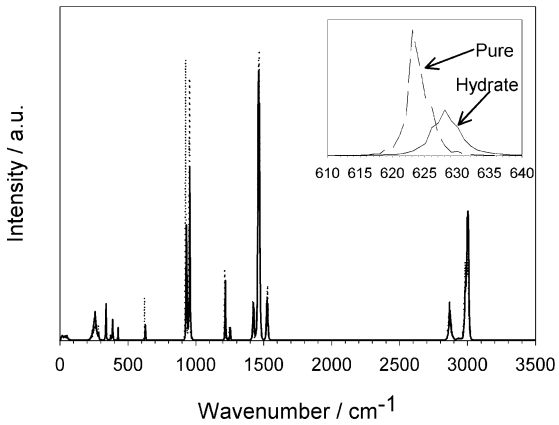

Figure 8. Simulated power spectrum of R141b in both the hydrate and (pure) gas phases. The inset shows the peak shift at 628 cm^{-1}.

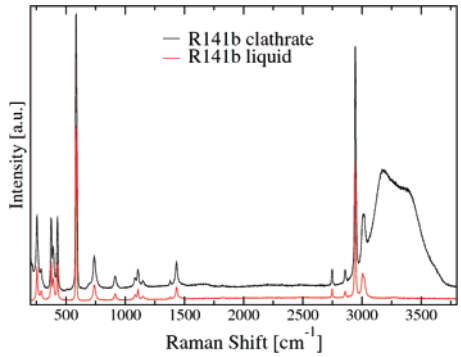

Figure 9. Raman spectra of R141b hydrate (black line) and liquid sample (red line) at 0 °C, using a 532 nm laser line. Peak shifts between the clathrate and liquid sample are below 1 cm^{-1}, except in the region near 586 cm^{-1} and above 2900 cm^{-1}, as discussed in the text.

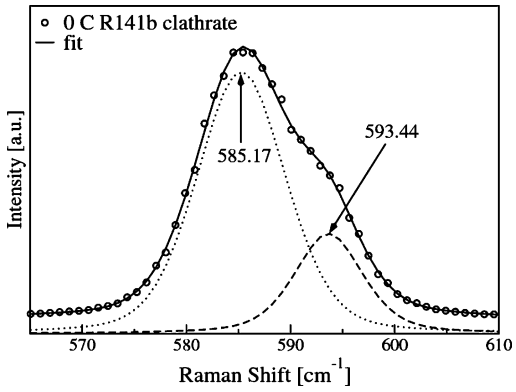

Figure 10. Peak splitting at 586 cm^{-1} in the R141b hydrate sample at 0 °C. Two pseudo-Voigt peaks (dashed line) were required for a satisfactory fit to the clathrate sample data. The liquid reference peak (dotted line) shows no splitting.

due to water molecules in R141b hydrate is very similar to that of hexagonal ice (Figure 7). However, for both the high- and low-frequency modes, the ice spectrum shows a more detailed structure. The water peaks are in relatively good agreement with the Raman peaks of hexagonal ice at −4 °C (3150−3375, 1640, and 600−870 cm^{-1}).[52] The increased rotational motion of water molecules in the hydrate phase compared to hexagonal ice may explain the difference in fine structure between 3600 and 3750 cm^{-1}.

A comparison of the R141b hydrate power spectrum with that of pure R141b is shown in Figure 8. For all bending and stretching modes that involve C−Cl or C−F bonds, hydrate peaks were shifted 5−10 cm^{-1} higher than those in pure R141b.

TABLE 4: Halogen−Water Coordination Numbers for Hydrates of 1 and 2 Measured at 3.0 Å

RDF pair[a]	R141b (**1**)	isomer (**2**)
Cl−H_w	0.12	0.17
F−H_w	0.06	0.11

[a] H_w and O_w refer to water H and O atoms, respectively.

TABLE 5: Fitted Peak Positions in R141b Hydrate and the Liquid R141b Reference at 0 °C

R141b hydrate		R141b liquid reference		
Raman shift (cm^{-1})	error	Raman shift (cm^{-1})	error	peak shift (cm^{-1})
255.75	0.06	255.99	0.05	−0.24
290.19	0.24	290.75	0.15	−0.56
374.81	0.04	374.67	0.04	0.14
392.04	0.09	392.75	0.10	−0.71
428.07	0.03	428.07	0.04	0.00
585.17	0.05	586.03	0.01	−0.86
593.44	0.10	586.03	0.01	7.42
740.00	0.09	740.23	0.10	−0.23
915.86	0.17	915.67	0.18	0.18
1082.96	0.30	1083.16	0.27	−0.20
1109.10	0.14	1108.26	0.11	0.84
1151.43	0.47	1150.94	0.43	0.49
1380.13	0.33	1380.21	0.39	−0.08
1433.48	0.10	1434.24	0.12	−0.76
2748.12	0.09	2747.66	0.10	0.46
2858.06	0.14	2857.73	0.17	0.33
2944.42	0.02	2943.24	0.02	1.18
3002.48	0.64	3004.68	0.29	−2.20
3017.39	1.05	3020.37	0.44	−2.98
3159.40	0.23			
3343.36	0.69			

Modes involving C−H bonds occur at identical frequencies in the two phases. No peak shifts were seen in the librational modes (<500 cm^{-1}), which indicates that the nonbonding environments experienced by R141b in the two phases are similar. Despite the presence of hydrogen bonds between halogen atoms and water molecules (Table 2), the overall hydrophobic effect of R141b surrounded by water molecules is a strengthening of intramolecular interactions (blue shift in bonded modes) with no change in intermolecular interactions.

Hydrate Synthesis and Characterization. The 0 °C Raman spectra for R141b hydrate and pure liquid R141b are shown in Figure 9. Table 5 shows the peak fit data and calculated peak shifts. The 586.03 cm^{-1} peak in the liquid reference spectrum is split in the hydrate, as shown in Figure 10. It was necessary to use two pseudo-Voigt peaks to obtain a satisfactory fit to this region of the hydrate spectrum, while the liquid reference spectrum was easily fitted with a single pseudo-Voigt peak. The most likely analogue to the 586.03 cm^{-1} peak in the Raman spectrum occurs in the computational spectra at 559 cm^{-1} (DFT, Figure 5) and 628 cm^{-1} (MD simulation, Figure 8). Analysis of atomic power spectra (data not shown) indicates that this peak is comprised of a mode involving C, Cl, and F atoms, but animation of the corresponding DFT peak indicates that this is primarily a symmetric carbon−halogen stretch mode. The hydrate peak is shifted approximately 7 cm^{-1} higher than the pure R141b peak in both computational calculations. As noted above, the confining effects of the water cage result in higher vibrational frequencies for bonded modes in the R141b spectrum.

The temperature-induced shift of the R141b liquid peak at 586 cm^{-1} is less than 0.3 cm^{-1} between −78 and 0 °C (data not shown). The splitting and relative shift of the peaks in the hydrate sample at this Raman shift are larger than 0.3 cm^{-1}

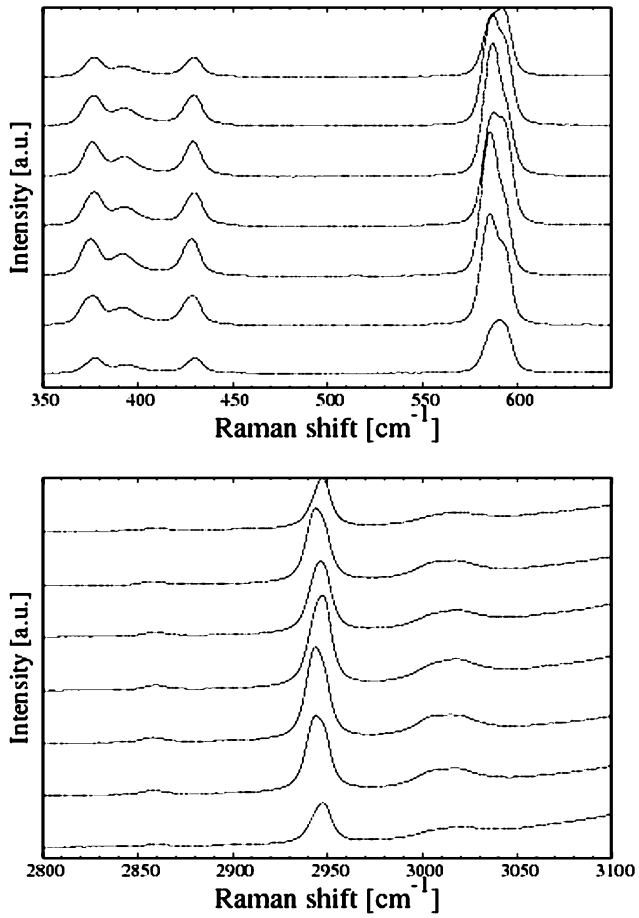

Figure 11. Raman spectra of R141b hydrate as a function of temperature at low frequencies (top) and high frequencies (bottom). The scan temperatures from bottom to top are −4, −2, 0, +1, +2, +3, and +4 °C, respectively. The peak at about 586 cm^{-1} (top) exhibits splitting and intensity variation, indicating that the associated molecular vibration is influenced by interactions with the cage. Peaks at higher frequency (bottom) are also shown.

(Figure 11) and may indicate small changes in the R141b vibration frequencies due to interactions with the cage walls. There was difficulty obtaining a good fit to the hydrate peaks at 3002 and 3017 cm^{-1} in the wavenumber regions corresponding to peaks at 3004.7 and 3020.4 cm^{-1} in the reference spectrum. The fitting difficulties in this region were due to the large signal in the hydrate sample from peaks at 3159 and 3343 cm^{-1}.

Conclusions

The thermodynamic properties of halogenated hydrocarbons and their hydrate formation make them good candidates for water desalination processes. We have carried out a combined computational and experimental study of hydrates formed from a prototype HCFC (hydrochlorofluorocarbon), R141b (**1**). Computational efforts were used to explain why **1** can form structure II hydrates at STP, but its isomer (**2**) cannot. Significant orbital overlap exists between **2** and water molecules in either small or large cages of structure II hydrates. Our orbital overlap results were verified by comparing molecular diameters using a contour method to map the DFT electron density. We plan to extend our method of calculating molecular diameters to update the tables of host diameters obtained from geometric and van der Waals radius considerations. It is important to note that the DFT calculations represent 0 K results and may be limited in extrapolation to real temperatures such as 265 K where the R141b hydrate is stable. Classical simulations (Figure 4) indicate that R141b molecules are in dynamical equilibrium with all water molecules in the large cage of the hydrate and are not fixed at any local coordination. Additionally, the *anti* and *gauche* isomers of **2** are found to have a relatively small energy barrier between conformers, and both can occur in the equilibrated systems.

X-ray diffraction results of R141b hydrate indicate a crystallography consistent with a structure II unit cell. Constant-pressure simulations show that R141b hydrates are stable at ambient pressure up to 265 K, which is slightly lower than but in good agreement with the experimental limit of 281.4 K.[6] Peaks in the Raman spectra were assigned on the basis of calculated vibrational spectra from DFT simulations. Of particular note is a shift in R141b vibrational modes between the liquid and hydrate phases. No shift is observed in the low-wavenumber librational modes, so the local (nonbonding) environments around R141b molecules in both phases are similar.

Acknowledgment. We acknowledge support from the Sandia National Laboratories under its LDRD program. Sandia is a multiprogram laboratory operated by Sandia Corp., a Lockheed Martin company, for the United States Department of Energy's National Nuclear Security Administration under Contract DE-AC04-94AL85000.

References and Notes

(1) Sloan, E. D., Jr. *Clathrate Hydrates of Natural Gases*; Marcel Dekker, Inc.: New York, 1998.
(2) Buffett, B. A. *Annu. Rev. Earth Planet. Sci.* **2000**, *28*, 477.
(3) Knox, W. G.; Hess, M.; Jones, G. E.; Smith, H. B. *Chem. Eng. Prog.* **1961**, *57*, 66.
(4) Barduhn, A. J.; Towlson, H. E.; Hu, Y. C. *AIChE J.* **1962**, *8*, 176.
(5) McCormack, R. A.; Niblock, G. A. *Investigation of high freezing temperature, zero ozone, and zero global warming potential, clathrate formers for desalination*; U.S. Department of the Interior, Bureau of Reclamation, Technical Service Center, Water Treatment Engineering and Research Group: Denver, CO, 2000.
(6) Brouwer, D. H.; Brouwer, E. B.; MacLaurin, G.; Lee, M.; Parks, D.; Ripmeester, J. A. *Supramol. Chem.* **1997**, *8*, 361.
(7) Akiya, T.; Shimazaki, T.; Oowa, M.; Matsuo, M.; Yoshida, Y. *Int. J. Thermophys.* **1999**, *20*, 1753.
(8) Liang, D.; Guo, K.; Wang, R.; Fan, S. *Fluid Phase Equilib.* **2001**, *187−188*, 61.
(9) Imai, S.; Okutani, K.; Ohmura, R.; Mori, Y. H. *J. Chem. Eng. Data* **2005**, *50*, 1783.
(10) Seitz, J. C.; Pasteris, J. D.; Wopenka, B. *Geochim. Cosmochim. Acta* **1987**, *51*, 1651.
(11) Sum, A. K.; Burruss, R. C.; Sloan, E. D. *J. Phys. Chem. B* **1997**, *101*, 7371.
(12) Uchida, T.; Hirano, T.; Ebinuma, T.; Narita, H.; Gohara, K.; Mae, S.; Matsumoto, R. *AIChE J.* **1999**, *45*, 2641.
(13) English, N. J.; MacElroy, J. M. D. *J. Comput. Chem.* **2003**, *24*, 1569.
(14) English, N. J.; Johnson, J. K.; Taylor, C. E. *J. Chem. Phys.* **2005**, *123*.
(15) Chialvo, A. A.; Houssa, M.; Cummings, P. T. *J. Phys. Chem. B* **2002**, *106*, 442.
(16) Greathouse, J. A.; Cygan, R. T.; Simmons, B. A. *J. Phys. Chem. B* **2006**, *110*, 6428.
(17) Cao, Z. T.; Tester, J. W.; Sparks, K. A.; Trout, B. L. *J. Phys. Chem. B* **2001**, *105*, 10950.
(18) Anderson, B. J.; Tester, J. W.; Trout, B. L. *J. Phys. Chem. B* **2004**, *108*, 18705.
(19) Vatamanu, J.; Kusalik, P. G. *J. Phys. Chem. B* **2006**, *110*, 15896.
(20) Forrisddahl, O. K.; Kvamme, B.; Haymet, A. D. J. *Mol. Phys.* **1996**, *89*, 819.
(21) Klauda, J. B.; Sandler, S. I. *Chem. Eng. Sci.* **2003**, *58*, 27.
(22) Rodger, P. M. *Ann. N. Y. Acad. Sci.* **2000**, *912*, 474.
(23) Moon, C.; Taylor, P. C.; Rodger, P. M. *J. Am. Chem. Soc.* **2003**, *125*, 4706.
(24) Storr, M. T.; Taylor, P. C.; Monfort, J. P.; Rodger, P. M. *J. Am. Chem. Soc.* **2004**, *126*, 1569.
(25) Nada, H. *J. Phys. Chem. B* **2006**, *110*, 16526.
(26) Alavi, S.; Ripmeester, J. A.; Klug, D. D. *J. Chem. Phys.* **2005**, *123*, 024507.

(27) Alavi, S.; Ripmeester, J. A.; Klug, D. D. *J. Chem. Phys.* **2006**, *124*, 014704.
(28) Klauda, J. B.; Sandler, S. I. *J. Phys. Chem. B* **2002**, *106*, 5722.
(29) Sluiter, M. H. F. B.; Rodion, V.; Jain, A.; Belosludov, V. R.; Adachi, H.; Kawazoe, Y.; Higuchi, K.; Otani, T. *Lect. Notes Comput. Sci.* **2003**, *2858*, 330.
(30) Dauber-Osguthorpe, P.; Roberts, V. A.; Osguthorpe, D. J.; Wolff, J.; Genest, M.; Hagler, A. T. *Proteins: Struct., Funct., Genet.* **1988**, *4*, 31.
(31) Bradshaw, R. W.; Simmons, B. A.; Majzoub, E. W.; Clift, W. M.; Dedrick, D. E. Clathrate Hydrates for Production of Potable Water. Materials Science of Water Purification, San Francisco, 2006.
(32) Ohmura, R.; Ogawa, M.; Yasuoka, K.; Mori, Y. *J. Phys. Chem. B* **2003**, *107*, 5289.
(33) Kobayashi, I.; Ito, Y.; Mori, Y. *Chem. Eng. Sci.* **2001**, *56*, 4331.
(34) Komiyama, M.; Kobayashi, M. *J. Phys. Chem. B* **1999**, *103*, 10651.
(35) Delley, B. *J. Chem. Phys.* **1990**, *92*, 508.
(36) Delley, B. *J. Chem. Phys.* **2000**, *113*, 7756.
(37) McMullan, R. K.; Kvick, A. *Acta Crystallogr., B* **1990**, *46*, 390.
(38) Perdew, J. P.; Wang, Y. *Phys. Rev. B* **1992**, *45*, 13244.
(39) Wilson, E. B.; Cross, P. C.; Decius, J. C. *Molecular Vibrations: The Theory of Infrared and Raman Vibrational Spectra*; Courier Dover: New York, 1980.
(40) Teleman, O.; Jonsson, B.; Engstrom, S. *Mol. Phys.* **1987**, *60*, 193.
(41) Frenkel, D.; Smit, B. *Understanding Molecular Simulation: From Algorithms to Applications*, 2nd ed.; Academic Press: San Diego, 2002.
(42) Glen, J. W. *Phys. Kondens. Mater.* **1968**, *7*, 43.
(43) McBride, C.; Vega, C.; Sanz, E.; MacDowell, L. G.; Abascal, J. L. F. *Mol. Phys.* **2005**, *103*, 1.
(44) Vega, C.; Sanz, E.; Abascal, J. L. F. *J. Chem. Phys.* **2005**, *122*.
(45) Young, D. C. *Computational Chemistry: A Practical Guide for Applying Techniques to Real World Problems*; John Wiley and Sons, Inc.: New York, 2001.
(46) Ruzsinszky, A.; Perdew, J. P.; Csonka, G. I. *J. Phys. Chem. A* **2005**, *109*, 11006.
(47) Tuma, C.; Sauer, J. *Phys. Chem. Chem. Phys.* **2006**, *8*, 3955.
(48) Hout, R. F.; Hehre, W. J. *J. Am. Chem. Soc.* **1983**, *105*, 3728.
(49) Davidson, D. W. Clathrate Hydrates. In *Water: A Comprehensive Treatise*; Franks, F., Ed.; Plenum Press: New York, 1973; Vol. 2, pp 130.
(50) Jeffrey, G. A.; Saenger, W. *Hydrogen Bonding in Biological Structures*; Springer-Verlag: New York, 1991.
(51) Nakanishi, K.; Solomon, P. H. *Infrared Absorption Spectroscopy*; Holden-Day: New York, 1977.
(52) Scherer, J. R.; Snyder, R. G. *J. Chem. Phys.* **1977**, *67*, 4794.